

Analyst

Accepted Manuscript



This is an *Accepted Manuscript*, which has been through the Royal Society of Chemistry peer review process and has been accepted for publication.

Accepted Manuscripts are published online shortly after acceptance, before technical editing, formatting and proof reading. Using this free service, authors can make their results available to the community, in citable form, before we publish the edited article. We will replace this *Accepted Manuscript* with the edited and formatted *Advance Article* as soon as it is available.

You can find more information about *Accepted Manuscripts* in the [Information for Authors](#).

Please note that technical editing may introduce minor changes to the text and/or graphics, which may alter content. The journal's standard [Terms & Conditions](#) and the [Ethical guidelines](#) still apply. In no event shall the Royal Society of Chemistry be held responsible for any errors or omissions in this *Accepted Manuscript* or any consequences arising from the use of any information it contains.

COMMUNICATION

Coumarin 545: an emission reference dye with a record-low temperature coefficient for ratiometric fluorescence based temperature measurements

Cite this: DOI: 10.1039/x0xx00000x

Received 00th January 2012,
Accepted 00th January 2012

Deqi Mao, ‡^{ab} Xiaogang Liu, ‡ §^c Qinglong Qiao,^{ab} Wenting Yin,^b Miao Zhao,^b Jacqueline M. Cole,^{*cd} Jingnan Cui,^{*a} and Zhaochao Xu^{*ab}

DOI: 10.1039/x0xx00000x

www.rsc.org/

The emission intensities of coumarin 545 solution exhibit a low temperature dependence, with a record-low temperature coefficient of only ~0.025% per °C. This monomer-aggregate coupled fluorescence system can be used for ratiometric temperature measurements with high spatial and temporal resolutions; three different working modes have been demonstrated.

Introduction

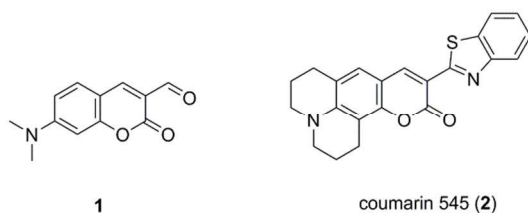
Temperature is a fundamental parameter affecting various physical and chemical processes;¹ fluorescent sensing of temperature has recently attracted considerable research interests across different fields,^{2, 3} such as tracking cellular events in biological systems^{4, 5} and exploring the flow mixing in fluid dynamics,^{6, 7} with high spatial and temporal resolutions. In most fluorescent systems, fluorescence intensities decrease with a rise in temperature owing to the thermal activation of nonradiative deexcitation pathways.^{2, 3, 7-14} Only polymer-based fluorescent thermometers have been reported with positive temperature coefficients (*i.e.*, stronger emission intensities at higher temperatures), because polymers offer a decreasing micro-environmental polarity around a polarity-sensitive fluorophore fragment at a higher temperature.¹⁵⁻¹⁷

The temperature dependence of fluorescence can be used to construct thermometers. In such applications, ratiometric measurements are preferred because it provides a built-in correction to permit signal ratioing and allow accurate and quantitative measurements.¹⁸ Ratiometric fluorescent thermometers usually contain one temperature-sensitive fluorophore as a sensor and one relatively temperature-insensitive fluorophore as a reference; the emission intensity ratios of the sensor and the reference afford temperature information.^{4, 18-22} However, the temperature “insensitive” reference fluorophores still exhibit rather high temperature coefficients. For example, Rhodamine 101, one of the most

commonly used reference dyes, possesses a temperature coefficient of 0.13% per °C at 20 °C, or ~5% intensity variation over a temperature change of 40 °C. Consequently, there is a strong need to develop new fluorescence systems with ultra-low temperature coefficients, for more accurate temperature measurements.

Aggregation of organic dyes in the solution phase is a frequently encountered phenomenon with profound implications on the photophysical, photochemical and biomedical properties of the dyes.²³⁻²⁶ J-aggregation leads to red-shifted and narrow absorption and fluorescence spectra, while H-aggregation causes blue-shifted and broadened absorption spectra. Making use of the molecular aggregation effects, we have recently proposed a design concept to achieve ultra-low temperature dependence of emission intensity using a monomer-aggregate coupled system.²⁷ Put simply, as the temperature goes up, the quantum efficiency of monomer emission decreases; while at the same time, the dissolution of aggregates boosts the quantity of monomers. By engineering a careful balance of these two factors, the overall monomer emission intensity could be maintained at a nearly constant level over different temperatures. Accordingly, a monomer-aggregate equilibrium system based on 7-(dimethylamino)-coumarin-3-carbaldehyde (**1**; Scheme 1) has demonstrated a low temperature coefficient, of only 0.05% per °C.

In this paper, coumarin 545 (**2**; Scheme 1) will be investigated along similar lines to **1**. It will be shown that **2** displays a record-low temperature coefficient, of only 0.025% per °C. More importantly, it will be demonstrated that **2** can act as a reference for Rhodamine 6G, resulting in a ratiometric fluorescent thermometer; compound **2** itself can also work as a ratiometric and self-calibrated fluorescent probe for temperature sensing, relying on different temperature dependence of the monomer and H-aggregate emissions.



Scheme 1. Molecular Structures of Studied Coumarin Derivatives.

Experimental Methods

Compound **2** was supplied by Exciton and used without further purification. UV–vis absorption spectra were collected on a Cary 60 UV–vis spectrophotometer. Fluorescence measurements were performed on an Agilent CARY Eclipse fluorescence spectrophotometer with a Single Cell Peltier temperature controller. For measurements of fluorescence decay dynamics, a pulsed diode laser of 405 nm was used as the excitation source. The emission of **2** was measured using a time-correlated single photon counting (TCSPC) setup from Edinburgh Instruments (OB 920). Fluorescent quantum yields were determined using Fluorescein as a reference. The quantum yield was calculated according to eq. 1:

$$\Phi_{F(x)} = \frac{I_s \int emission_x (n_x)^2}{I_x \int emission_s (n_s)^2} \Phi_{F(s)} \quad (\text{eq. 1})$$

where Φ_F represents the fluorescence quantum efficiency, I the absorbance at the excitation wavelength, $\int emission$ the area under the fluorescence spectrum, and n the refractive index of the solvents in use. Subscripts s and x indicate the reference standard and the unknown, respectively.

Results and Discussion

H-aggregation of coumarin 545

Before considering the low-temperature dependence merits and applications of a monomer-aggregate coupled system of **2**, its aggregation characteristics needed to be discerned. The UV–vis absorption, emission and fluorescence excitation spectra of **2** (Fig. 1) have been probed in five commonly used “good” solvents with varied polarities: methanol, tetrahydrofuran (THF), ethyl acetate (EA), dimethylformamide (DMF) and dimethyl sulfoxide (DMSO). H-aggregation of **2** was identified from the spectra in all five studied solvents.

The presence of H-aggregates in a solution of **2** is quite subtle. For example, the normalised UV–vis absorption spectra of **2** in methanol at various concentrations (from 1.5 to 30 μM) match each other very well (Fig. 1a, b); the correlation between the peak absorbance and the concentration of **2** closely follows the Beer-Lambert law (Fig. S1). Similarly, the normalised steady-state fluorescence spectra are independent of excitation wavelength (λ_{ex}) and top out at 520 nm when $\lambda_{\text{ex}} \geq 420$ nm (Fig. 1c, d). However, an unusual emission shoulder becomes obvious between 440 and 500 nm where $\lambda_{\text{ex}} \leq 410$ nm. The short wavelength emission (*i.e.*, at $\lambda_{\text{em}} = 470$ nm) corresponds to a fluorescence excitation spectrum peaking at ~ 400 nm, in

contrast to that of ~ 475 nm for the long wavelength emission (Fig. 1g, h). These exceptional spectral profiles clearly indicate the presence of more than one species in the solution, and lead to the identification of molecular aggregates of **2**.

The primary emission peak at 520 nm has been attributed to monomers of **2**. Assigning this peak to J-aggregate formation was not tenable because the lifetimes of J-aggregates, where present, are typically shorter than those of monomers. Fluorescent lifetime measurements showed that the lifetime of long wavelength emission in the solution of **2** is greater than that of the blue-shifted secondary emission shoulder, when excited at 405 nm (Table S1). The dominant presence of monomers is understandable, considering that **2** exhibits good solubility in methanol, and the 520 nm emission peak is predominant even at a very low dye concentration (*i.e.*, $[2] = 1.5 \mu\text{M}$). Accordingly, the blue-shifted secondary emission shoulder is assigned to H-aggregates of **2**.

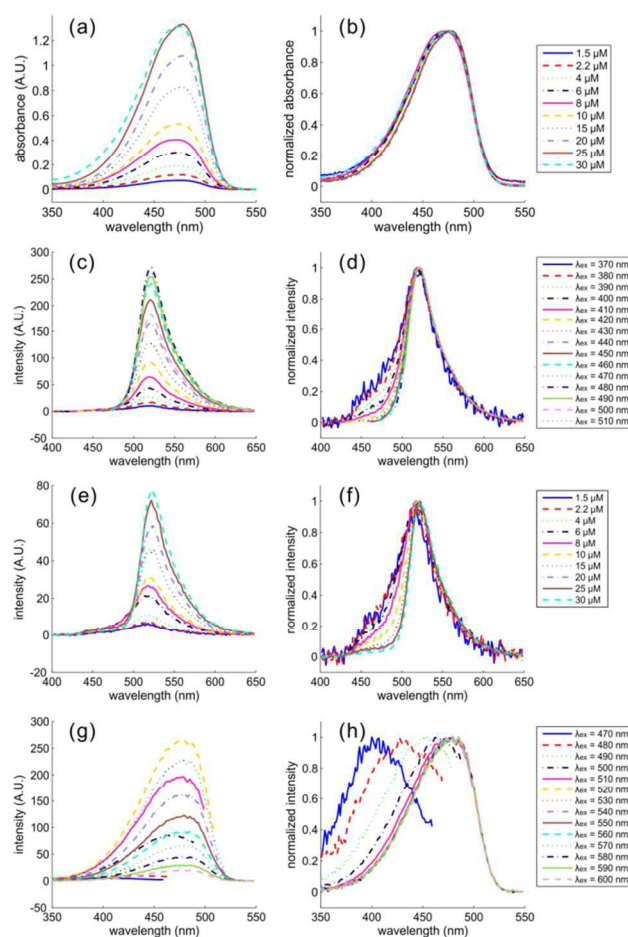


Fig. 1. (a) UV–vis absorption spectra of **2** in methanol at various concentrations from 1.5 to 30 μM ; (c) fluorescence spectra of **2** ($[2] = 8 \mu\text{M}$) in methanol, excited at various wavelengths from 370 to 510 nm; (e) fluorescence spectra of **2** in methanol at various concentrations from 1.5 to 30 μM , excited at 390 nm; (g) fluorescence excitation spectra of **2** ($[2] = 8 \mu\text{M}$) in methanol, monitored at various emission wavelengths from 470 to 600 nm. (b), (d), (f), and (h) correspond to the normalised spectra in (a), (c), (e), and (g), respectively.

Interestingly, although the fluorescence decay dynamics of **2** at various emission wavelengths (from 450 to 600 nm at a step

size of 10 nm) can all be described reasonably well by a single-exponential decay function, the extracted lifetime constant first stabilizes at ~ 2.71 ns (for $\lambda_{\text{em}} < 460$ nm) and then gradually increases to the point of saturation reached by ~ 3.13 ns (for $\lambda_{\text{em}} > 560$ nm; Table S1). These two stable time constants are related to H-aggregate and monomer emissions, respectively. Intermediate lifetime values should arise from a mixture of H-aggregate and monomer emission contributions. By remodeling the fluorescence decay dynamics in the transitional region using double-exponential functions (with two fixed time constants of 2.71 and 3.13 ns), the contributions of both H-aggregate and monomer emissions can be determined (Table S2). Based on the models of varied contributions at different emission wavelengths and the overall emission spectrum, it was possible to trace out the monomer and aggregate emission spectra (Fig. 2). It is worth noticing that the H-aggregate emission spectrum is broader and has a larger Stokes shift (~ 100 nm) than that of monomer emission (~ 45 nm).

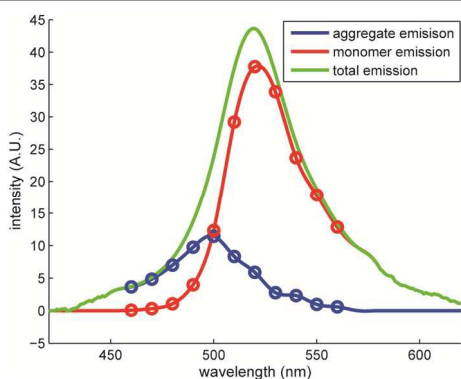


Fig. 2. Calculated fluorescent spectra of H-aggregates and monomers of **2** in methanol ($\lambda_{\text{ex}} = 405$ nm, $[\mathbf{2}] = 8 \mu\text{M}$). These profiles were generated by tracing out a series of modelled fluorescent decay dynamics.

As the concentration of **2** increases, one might expect that more H-aggregates form. However, the associated H-aggregate emission in the normalised emission spectra becomes less significant between 440 to 500 nm (Fig. 1e, f). This extraordinary phenomenon can be rationalized by two factors. Firstly, the emission in this region matches the UV–vis absorption spectrum of **2** and could be re-absorbed (*via* the so-called inner-filter effect).²⁸ Secondly, the size of H-aggregates grows (from dimers to high-order aggregates) as the concentration of **2** rises, and the quantum efficiencies decrease accordingly.

The presence of H-aggregates is also found in solutions of **2** with THF, EA, DMF or DMSO (Fig. S2–S5).

The temperature dependence of the fluorescence intensities of **2**

The monomer-aggregate coupled system of **2** possesses a unique temperature dependence (Fig. 3; Table S3). While excited at 390 nm in methanol, where strong absorption is observed owing to H-aggregates, the fluorescence intensity unusually exhibits an increase with rising temperature (Fig. 3a). This is likely caused by the dissolution of high-order H-aggregates, forming more low-order H-aggregates with higher

quantum efficiencies. While the quantity of monomers also increases with temperature, this increase cannot completely compensate for the quantum efficiency drop of monomer emission. For instance, while excited at 490 nm, where the monomers strongly absorb, the emission intensity of **2** possesses a negative temperature coefficient (Fig. 3c). In contrast, by choosing an intermediate, or “optimal”, excitation wavelength, *i.e.*, 430 nm, the overall emission intensities of this system remain little changed, by a balance act between the intensification of the H-aggregate emission and the decrease in monomer emission. Consequently, the intensity of this fluorescence system exhibits a small variation of only $\sim 1\%$ over a temperature change of 40 °C, or a record-low effective temperature coefficient of $\sim 0.025\%$ per °C (Fig. 3b); the peak emission wavelength is shifted by only 2 nm. It should be pointed out that λ_{ex} was varied at a step size of 10 nm during the search of the “optimal” excitation wavelength; it is reasonable to expect an even lower temperature coefficient close to 0, by reducing the step size of λ_{ex} .

At $\lambda_{\text{ex}} = 430$ nm, the molar absorptivity of **2** amounts to $2.7 \times 10^4 \text{ L mol}^{-1} \text{ cm}^{-1}$ and the overall fluorescence quantum efficiency is 78%, indicating good emission brightness in methanol.

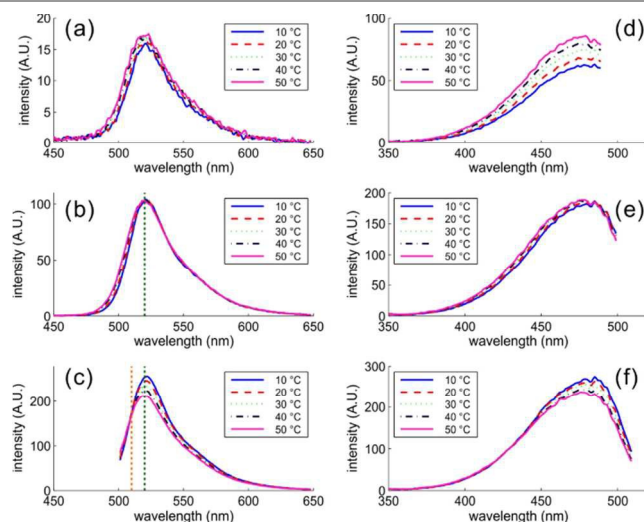


Fig. 3. Fluorescence spectra of **2** in methanol excited at (a) 390 nm, (b) 430 nm and (c) 490 nm; fluorescence excitation spectra of **2** in methanol monitored at the emission wavelengths of (d) 500 nm, (e) 510 nm and (f) 520 nm. $[\mathbf{2}] = 8 \mu\text{M}$. Three vertical lines at 510 and 520 nm are drawn in (c) and (d) to illustrate the different temperature sensitivities of the corresponding emission intensities.

This balance act is further corroborated by probing the fluorescence excitation spectra. At an intermediate emission wavelength (*i.e.*, $\lambda_{\text{em}} = 510$ nm), the corresponding fluorescence excitation spectrum exhibits almost no change from 10 °C to 40 °C (Fig. 3e). As λ_{em} is blue-shifted, where the contribution of H-aggregate emission becomes higher, the fluorescent excitation spectrum rises with temperature (Fig. 3d). This rise reflects the increasing quantum efficiency of H-aggregates. In contrast, the decreasing monomer quantum efficiency is demonstrated by the declining fluorescence excitation spectrum

while monitored at a longer emission wavelength (*i.e.*, $\lambda_{em} = 520$ nm; Fig. 3f).

Similar temperature dependence and bright fluorescence were also observed when **2** was dissolved in THF, EA, DMF and DMSO, with temperature coefficients at the corresponding “optimal” excitation wavelengths, measured as 0.025%, 0.029%, -0.043% and -0.044% per °C, respectively (Fig. S6—S10; Table S3—S5).

The concentration dependence of the “optimal” excitation wavelengths has also been investigated. Since the monomer-aggregate equilibrium is concentration dependent, a shift in the optimal excitation wavelength is expected.²⁷ Nevertheless, such shifts are generally small, owing to the relatively subtle presence of H-aggregates in the solution of **2**. For example, the optimal excitation wavelength remains at 420 nm as [2] increases from 5 to 20 μ M in DMF; it shifts to 430 nm as [2] decreases to 1 or 2 μ M (Table S5). This weak concentration dependence suggests that a fixed excitation wavelength can be used to achieve temperature insensitivities of fluorescence intensities in **2**, over a wide concentration range.

It is worth highlighting that the emission intensity of **2** exhibits a higher degree of temperature insensitivity than that of **1**. For example, the effect of temperature insensitive fluorescence intensities was observed only in THF (and other solvents of similar polarities), but not in methanol and DMSO for **1**. In contrast, this effect was noticed in all five solvents (including THF, EA, DMF, methanol and DMSO) for **2**. Moreover, the lowest temperature coefficient of **1** was measured at 0.05% per °C, with a blue shift in the peak emission wavelength by 5 nm from 5 to 50 °C. In contrast, the temperature coefficient of **2** is as low as 0.025% per °C, and the maximum emission wavelength is shifted by only 2 nm from 10 to 50 °C.²⁷

The applications of **2** in fluorescent thermometers

Its uniquely low temperature dependence makes **2** a strong candidate for fluorescent temperature sensing applications. Three different working modes are now demonstrated.

In the first mode, the solution of **2** is excited at the “optimal” excitation wavelength, serving as a reference dye, in conjunction with another temperature sensitive dye, such as Rhodamine 6G (Fig. 4). When the mixture of **2** and Rhodamine 6G was excited at 460 and 540 nm, respectively, the resulting emission at 520 (from **2**) and 567 nm (mainly from Rhodamine 6G) exhibit different temperature sensitivities (Fig. 4a). Consequently, the ratios of the emission intensities at these two wavelengths can be used to construct a calibration curve and afford temperature information (Fig. 4b).

It is interesting to point out that Förster resonance energy transfer (FRET) from **2** to Rhodamine 6G occurs in this mixture. The UV—vis absorption spectrum of Rhodamine 6G (represented by the grey shadowed area in Fig. 4a) matches the emission spectrum of **2** very well. Consequently, the emission at 567 nm consists of contributions from both **2** (~70%) and Rhodamine 6G (~30%), at $\lambda_{ex} = 460$ nm; in the emission of Rhodamine 6G, ~25% is from direct excitation, and ~75% via FRET.

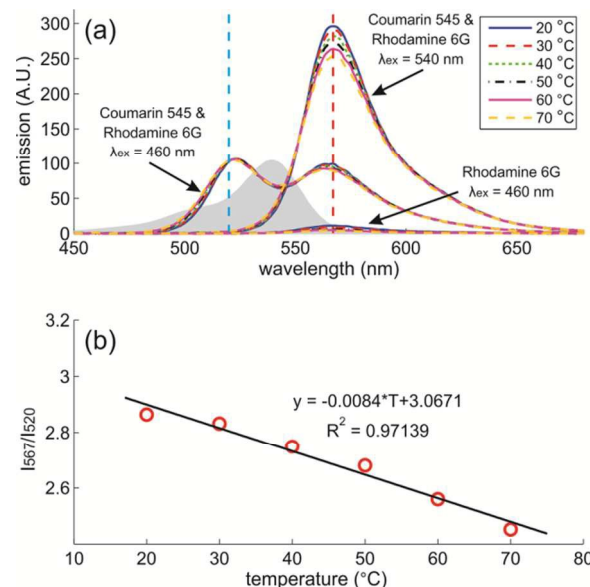


Fig. 4. (a) The emission spectra of a mixture of **2** and/or Rhodamine 6G ([2] = [Rhodamine 6G] = 8 μ M) in DMSO at various temperatures, excited at 460 and 540 nm, respectively. Two vertical lines at 520 and 567 nm are drawn to illustrate the different temperature sensitivities of the corresponding emission intensities. (b) Temperature dependence of the ratios of fluorescence intensities in DMSO at 567 and 520 nm (excited at 540 and 460 nm, respectively), and the associated best-fit equation.

In the second and the third modes, no other dye is required. When the solution of **2** is excited at different wavelengths (*i.e.*, 430 and 490 nm), the long-wavelength emission of **2** (*i.e.*, 520 nm) displays different temperature sensitivities, owing to a manifestation of different contributions from the H-aggregate and monomer emissions (Fig. 3b, c). As a result, the ratios of emission intensities at 520 nm, excited at 430 and 490 nm, respectively, can be used to derive temperature information (Fig. 5a).

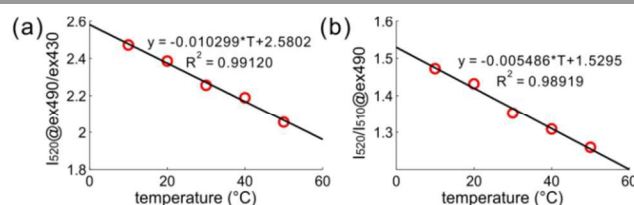


Fig. 5. Temperature dependence of (a) the ratios of fluorescence intensities of **2** in methanol at 520 nm, excited at 490 and 430 nm, respectively, and the associated best-fit equation; (b) the ratios of fluorescence intensities of **2** in methanol at 520 and 510 nm, excited at 490 nm, and the associated best-fit equation. [2] = 8 μ M.

Similarly, when the monomer-aggregate coupled system of **2** is excited at 490 nm, the emission spectrum exhibits a different temperature dependence at 510 and 520 nm (Fig. 3c). Hence, the ratios of emission intensities at 510 and 520 nm, can be used for ratiometric temperature measurements in the third mode (Fig. 5b).

Similar ratiometric temperature calibration curves can also be constructed in other solvents, such as THF (Fig. S11) and DMSO (Fig. S12). Note that the ratiometric temperature

1 calibration curves are slightly concentration-dependent (Fig.
2 S12 and S13). However, this problem may be circumvented in a
3 closed system, where [2] can be accurately controlled.

4 Conclusion

5 The existence of H-aggregation in a solution of coumarin 545
6 (**2**) has been revealed. This monomer-aggregate coupled system
7 demonstrates a unique temperature dependence. As the
8 temperature increases, the H-aggregate emission intensifies,
9 while the monomer emission decreases slightly. By choosing an
10 intermediate excitation wavelength and balancing the
11 contributions of monomer and H-aggregate emissions, the
12 fluorescence intensity of **2** remains little varied over a
13 temperature change of 40 °C, resulting in a record-low
14 temperature coefficient of 0.025% per °C in methanol. Similar
15 effects are also observed in other solvents, such as THF, EA,
16 DMF and DMSO. This fluorescence system can thus be used as
17 a temperature-insensitive reference. Moreover, based on the
18 unique temperature dependent emission of **2**, ratiometric
19 temperature measurements can be performed, either in
20 conjunction with another highly temperature-sensitive dye, or
21 by exploring different temperature sensitivities of the monomer
22 and H-aggregate emissions. This study has significant
23 implications to the development of fluorescence based
24 thermometer.

25 Acknowledgment

26 X.L. is grateful to Singapore Economic Development Board for
27 a Clean Energy Scholarship. W.T. is supported by the National
28 Natural Science Foundation of China (21402191). J.M.C.
29 thanks the Fulbright Commission for a UK-US Fulbright
30 Scholar Award, hosted by Argonne National Laboratory where
31 work done was supported by DOE Office of Science, Office of
32 Basic Energy Sciences, under contract No. DE-AC02-
33 06CH11357. J.C. and Z.X. acknowledge financial support from
34 the National Natural Science Foundation of China (21276251),
35 Ministry of Human Resources and Social Security of PRC, the
36 100 talents program funded by Chinese Academy of Sciences,
37 State Key Laboratory of Fine Chemicals of China (KF1105)
38 and the National Science Fund for Excellent Young Scholars
39 (21422606).

40 Notes and references

41 ^a State Key Laboratory of Fine Chemicals, Dalian University of Technology,
42 Dalian 116012, China.

43 ^b Key Laboratory of Separation Science for Analytical Chemistry, Dalian
44 Institute of Chemical Physics, Chinese Academy of Sciences, Dalian 116023,
45 China.

46 ^c Cavendish Laboratory, Department of Physics, University of Cambridge, J.
47 Thomson Avenue, Cambridge, CB3 0HE, UK.

48 ^d Argonne National Laboratory, 9700 S Cass Avenue, Argonne, IL 60439,
49 USA.

50 Corresponding Author

51 E-Mail: zcxu@dicp.ac.cn; jncui@dlut.edu.cn; jmc61@cam.ac.uk. Tel: +86-
52 411-84379648. Fax: +86-411-84379648.

† Electronic Supplementary Information (ESI) available: molecular
structures of studied coumarins; the UV-vis absorption, emission and
fluorescence excitation spectra of **2** in THF and DMSO, at various
concentrations and temperatures; the single/double-exponential fitting
parameters to the fluorescence decay dynamics of **2** in methanol;
temperature calibration curves based on the ratiometric fluorescence
measurements of **2** in THF and DMSO. See DOI: 10.1039/b000000x/

‡ These authors contributed equally.

§ Current address: Singapore-MIT Alliance for Research and
Technology (SMART) Centre, 1 CREATE Way, Singapore 138602,
Singapore.

1. G. Kucsko, P. C. Maurer, N. Y. Yao, M. Kubo, H. J. Noh, P. K. Lo,
H. Park and M. D. Lukin, *Nature*, 2013, 500, 54-58.
2. X. D. Wang, O. S. Wolfbeis and R. J. Meier, *Chem. Soc. Rev.*, 2013,
42, 7834-7869.
3. Z. Yang, J. Cao, Y. He, J. H. Yang, T. Kim, X. Peng and J. S. Kim,
Chem. Soc. Rev., 2014, 43, 4563-4601.
4. S. Kiyonaka, T. Kajimoto, R. Sakaguchi, D. Shinmi, M. Omatsu-
Kanbe, H. Matsuura, H. Imamura, T. Yoshizaki, I. Hamachi, T.
Morii and Y. Mori, *Nat. Methods*, 2013, 10, 1232-1238.
5. K. Okabe, N. Inada, C. Gota, Y. Harada, T. Funatsu and S.
Uchiyama, *Nat. Commun.*, 2012, 3, 705.
6. C. Gosse, C. Bergaud and P. Low, in *Thermal Nanosystems and
Nanomaterials*, ed. S. Volz, 2009, 118, 301-341.
7. S. Ryu, I. Yoo, S. Song, B. Yoon and J. M. Kim, *J. Am. Chem. Soc.*,
2009, 131, 3800-3801.
8. T. Ozawa, H. Yoshimura and S. B. Kim, *Anal. Chem.*, 2013, 85, 590-
609.
9. Y. Jiang, X. Yang, C. Ma, C. Wang, Y. Chen, F. Dong, B. Yang, K.
Yu and Q. Lin, *ACS Appl. Mater. Interfaces*, 2014, 6, 4650-
4657.
10. J. Feng, K. Tian, D. Hu, S. Wang, S. Li, Y. Zeng, Y. Li and G. Yang,
Angew. Chem., Int. Ed., 2011, 50, 8072-8076.
11. V. F. Pais, J. M. Lassaletta, R. Fernandez, H. S. El-Sheshtawy, A.
Ros and U. Pischel, *Chemistry (Weinheim an der Bergstrasse,
Germany)*, 2014, 20, 7638-7645.
12. N. Chandrasekharan and L. A. Kelly, *J. Am. Chem. Soc.*, 2001, 123,
9898-9899.
13. S. L. Shinde and K. K. Nanda, *Angew. Chem., Int. Ed.*, 2013, 52,
11325-11328.
14. Z. Gan, X. Wu, J. Zhang, X. Zhu and P. K. Chu, *Biomacromolecules*,
2013, 14, 2112-2116.
15. C. Gota, K. Okabe, T. Funatsu, Y. Harada and S. Uchiyama, *J. Am.
Chem. Soc.*, 2009, 131, 2766-2767.
16. S. Uchiyama, N. Kawai, A. P. de Silva and K. Iwai, *J. Am. Chem.
Soc.*, 2004, 126, 3032-3033.
17. S. Uchiyama, Y. Matsumura, A. P. de Silva and K. Iwai, *Anal.
Chem.*, 2004, 76, 1793-1798.
18. E. J. McLaurin, L. R. Bradshaw and D. R. Gamelin, *Chem. Mater.*,
2013, 25, 1283-1292.
19. Y. Takei, S. Arai, A. Murata, M. Takabayashi, K. Oyama, S.
Ishiwata, S. Takeoka and M. Suzuki, *ACS Nano*, 2014, 8, 198-
206.
20. F. Ye, C. Wu, Y. Jin, Y. H. Chan, X. Zhang and D. T. Chiu, *J. Am.
Chem. Soc.*, 2011, 133, 8146-8149.

COMMUNICATION

Journal Name

- 1
2
3
4
5
6
7
8
9
10
11
12
13
14
15
16
17
18
19
20
21
22
23
24
25
26
27
28
29
30
31
32
33
34
35
36
37
38
39
40
41
42
43
44
45
46
47
48
49
50
51
52
53
54
55
56
57
58
59
60
21. A. E. Albers, E. M. Chan, P. M. McBride, C. M. Ajo-Franklin, B. E. Cohen and B. A. Helms, *J. Am. Chem. Soc.*, 2012, 134, 9565-9568.
 22. T. Kan, H. Aoki, N. Binh-Khiem, K. Matsumoto and I. Shimoyama, *Sensors (Basel, Switzerland)*, 2013, 13, 4138-4145.
 23. Z. Chen, A. Lohr, C. R. Saha-Moller and F. Wurthner, *Chem. Soc. Rev.*, 2009, 38, 564-584.
 24. F. Wurthner, T. E. Kaiser and C. R. Saha-Moller, *Angew. Chem., Int. Ed.*, 2011, 50, 3376-3410.
 25. X. Liu, J. M. Cole, P. Chow, L. Zhang, Y. Tan and T. Zhao, *J. Phys. Chem. C*, 2014, 118, 13042-13051.
 26. X. Liu, J. M. Cole and K. S. Low, *J. Phys. Chem. C*, 2013, 117, 14723-14730.
 27. X. Liu, D. Mao, J. M. Cole and Z. Xu, *Chem. Commun. (Camb)*, 2014, 50, 9329-9332.
 28. S. Fery-Forgues and D. Lavabre, *J. Chem. Educ.*, 1999, 76, 1260.